Sheffield Hallam University

Plasma analysis of Inductively Coupled Impulse Sputtering of Cu, Ti and Ni

LOCH, Daniel <http://orcid.org/0000-0003-3252-0142>, ARANDA GONZALVO, Yolanda and EHIASARIAN, Arutiun <http://orcid.org/0000-0001-6080-3946>

Available from Sheffield Hallam University Research Archive (SHURA) at:

http://shura.shu.ac.uk/9098/

This document is the author deposited version. You are advised to consult the publisher's version if you wish to cite from it.

Published version

LOCH, Daniel, ARANDA GONZALVO, Yolanda and EHIASARIAN, Arutiun (2017). Plasma analysis of Inductively Coupled Impulse Sputtering of Cu, Ti and Ni. Plasma Sources Science and Technology, 26 (6).

Repository use policy

Copyright © and Moral Rights for the papers on this site are retained by the individual authors and/or other copyright owners. Users may download and/or print one copy of any article(s) in SHURA to facilitate their private study or for non-commercial research. You may not engage in further distribution of the material or use it for any profit-making activities or any commercial gain.

Sheffield Hallam University Research Archive
http://shura.shu.ac.uk

IOPscience iopscience.iop.org

Plasma analysis of inductively coupled impulse sputtering of Cu, Ti and Ni

This content has been downloaded from IOPscience. Please scroll down to see the full text.

View the table of contents for this issue, or go to the journal homepage for more

Download details:

IP Address: 143.52.35.163
This content was downloaded on 16/06/2017 at 11:32

Please note that terms and conditions apply.

2017 Plasma Sources Sci. Technol. 26 065012

OPEN ACCESS
IOP Publishing

Plasma Sources Science and Technology

Plasma Sources Sci. Technol. **26** (2017) 065012 (12pp) https://doi.org/10.1088/1361-6595/aa6f79

Plasma analysis of inductively coupled impulse sputtering of Cu, Ti and Ni

D A L Loch[1], Y Aranda Gonzalvo[2,3] and A P Ehiasarian[1]

[1] Sheffield Hallam University, HIPIMS Technology Centre, Howard Street, Sheffield, United Kingdom
[2] HIDEN Analytical Ltd, Europa Boulevard, Warrington, United Kingdom
[3] Department of Mechanical Engineering, University of Minnesota, 111 Church Street SE, Minneapolis, United States of America

E-mail: d.loch@shu.ac.uk

Received 13 July 2016, revised 16 March 2017
Accepted for publication 26 April 2017
Published 17 May 2017

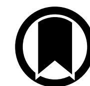

Abstract

Inductively coupled impulse sputtering (ICIS) is a new development in the field of highly ionised pulsed PVD processes. For ICIS the plasma is generated by an internal inductive coil, replacing the need for a magnetron. To understand the plasma properties, measurements of the current and voltage waveforms at the cathode were conducted. The ion energy distribution functions (IEDFs) were measured by energy resolved MS and plasma chemistry was analysed by OES and then compared to a model. The target was operated in pulsed DC mode and the coil was energised by pulsed RF power, with a duty cycle of 7.5%. At a constant pressure (14 Pa) the set peak RF power was varied from 1000–4000 W. The DC voltage to the target was kept constant at 1900 V. OES measurements have shown a monotonic increase in intensity with increasing power. Excitation and ionisation processes were single step for ICIS of Ti and Ni and multi-step for Cu. The latter exhibited an unexpectedly steep rise in ionisation efficiency with power. The IEDFs measured by MS show the material- and time-dependant plasma potential in the range of 10–30 eV, ideal for increased surface mobility without inducing lattice defects. A lower intensity peak, of high energetic ions, is visible at 170 eV during the pulse.

Keywords: ICIS, pulsed plasma, magnetron free sputtering, IEDF, OES, I-PVD

1. Introduction

Highly ionised plasma processes have helped to improve coating properties by enabling the control of the flux of ionised sputtered species, initially with an ancillary ionisation source such as inductively coupled plasma and magnetron sputtering (ICP-MS) [1] and more recently by utilising a higher pulsed power applied directly to a magnetron cathode such as high power impulse magnetron sputtering (HIPIMS) [2].

Deposition of magnetic materials, such as nickel, is problematic with magnetron sputtering as the magnetic confinement field that enhances the sputter process is reduced due to quenching of the magnetic flux density by the target material [3]. Additionally, depending on the magnetic configuration, conventional magnetron systems have target utilisation rates in the range between 38% and 63% [4].

ICP-MS is largely ICP assisted sputtering where the discharge on the cathode is created conventionally by means of DC or RF magnetron sputtering coupled with an additional external [5, 6] or immersed [7, 8] RF driven ICP coil to create a highly ionised plasma. The main ionisation mechanism is Penning ionisation for low electron densities and changes to electron-impact ionisation for high electron densities [9] as ICP processes produce ions of the sputtered material and are generally known as ionised PVD (I-PVD) processes.

In conventional magnetron sputtering the main ionisation mechanism for low to moderate pressures is electron impact as density of the sputtered species is related to the applied current and the sputter yield and the ionisation is related to the density of sputtered species, electron density and ionisation cross section [10].

The dominant ionisation mechanism is determined by the mean free path and ionisation cross section; electron collision

Original content from this work may be used under the terms of the Creative Commons Attribution 3.0 licence. Any further distribution of this work must maintain attribution to the author(s) and the title of the work, journal citation and DOI.

ionisation is more likely at high plasma density and low pressure, whereas Penning is favoured at low plasma densities and high pressures. For highly ionised I-PVD processes with an electron density larger than 10^{11} cm^{-3} at pressures up to 7 Pa, the dominant ionisation mechanism is electron collision due to the higher electron densities where Penning ionisation is less effective [9, 11].

Inductively coupled impulse sputtering (ICIS) enables the removal of the confining permanent magnetic field from the vicinity of the cathode [12]. To generate the plasma, pulsed RF power with density exceeding 20 W cm^{-2} is applied to an internal coil. Ar ions are attracted to the target surface by utilising high power DC pulses on the cathode and initiate sputtering. The sputtered material is then ionised as it passes through the coil volume, creating a highly ionised metal flux to the substrate. This high ionisation degree allows the coating of structured surfaces with high aspect ratios with a reduced lattice defect density [13, 14].

For ICIS the ionisation mechanisms and how the ionisation relates to the power input to the coil and the operating pressures is unclear and will be investigated in this paper.

To characterise the discharge properties, a series of experiments including current and voltage measurements at the coil and pulsed DC power supply, optical emission spectrographic measurements and energy-resolved mass spectroscopy of the plasma were conducted. The results of the plasma diagnostic measurements were reconciled with a model that correlates the increase of optical emission intensity to the power applied to the cathode. Three materials, copper, titanium and nickel, have been chosen for this study to investigate the material influence on the plasma. Nickel is especially of interest as it is a pure ferromagnetic material.

2. Experimental details

In ICIS technology, the primary plasma is created within the induction coil. The only magnetic field present is that which is established by the inductive coil perpendicular to the target surface, enabling highly ionised sputtering of magnetic material.

The coil of the ICIS system is a 2-turn 80 mm diameter made of solid copper rod (shown schematically in figure 1 and dimensions in table 1), assembled to a vacuum feed-through inside the UHV chamber (Kurt J Lesker CMS—18). The coil is connected to a Hüttinger PFG 5000 RF power supply (13.56 MHz) in pulse mode via a Hüttinger PFM 1500 A automatic matching network.

The cathode is magnet-free, 75 mm diameter and connected to a Hüttinger HIPIMS power supply HMP 6/16 which supplies a pulsed DC voltage. As the current drain at the target was small, a constant voltage determined by the setpoint of the HIPIMS generator was present on the target. Copper, titanium and nickel were used as sputtering targets. The working gas was argon.

Current and voltage measurements for the RF coil were taken at a location between the matching network and the vacuum feed through by a Tektronix P5100 100:1 voltage

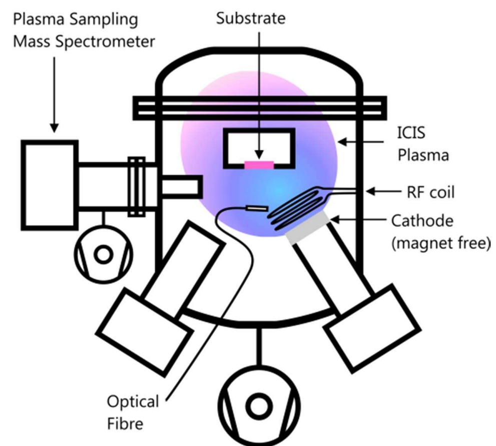

Figure 1. Experimental setup for ICIS plasma measurements inside the UHV system.

Table 1. Dimensions of the ICIS coil inside the UHV chamber.

Diameter of copper coil:	80 mm
Coil length:	25 mm
Cu rod diameter	5 mm
Number of turns:	2
Calculated inductance	0.44 μH
Effective series reactance (13.56 MHz)	37.4 Ohm
RF coil (centre) to substrate distance:	127 mm
Target to substrate distance:	130 mm

probe and a Tektronix P6021 AC 10:1 current probe. The current and voltage measurement for the target was taken at the HIPIMS power supply by voltage readout of the power supply and Pearson Current Monitor Model 110. All four channels were measured simultaneously by a Tektronix DPO 7054 4-channel oscilloscope. The probes were not calibrated for time response and delay times [15] and thus could not provide the absolute phase or instantaneous peak power; however the measurements were proportional to the actual values.

Information on the phase and impedance was gained with an Impedans OCTIV VI probe. This probe was also setup between the matching network and the vacuum feed through. Current, voltage, impedance, phase (represented as current in relation to voltage) and instantaneous power were measured simultaneously.

Measurements were taken for increasing peak RF power applied to the coil ranging from 1000–4000 W set at the power supply. A constant DC voltage of 1900 V was applied to the cathode. Constant pulse parameters of 500 Hz repetition frequency with a pulse width of 150 μs were applied, equivalent to a duty cycle of 7.5%. In view of the pulsing the average power dissipation in the coil was <360 W indicating a low thermal load. Argon was used as process gas resulting in a working pressure of 14 Pa.

The base pressure of the vacuum system was in the region of 5×10^{-7} Pa.

For the time resolved MS measurements, we have utilised 1 ms pulses with a frequency of 150 Hz resulting in a pulse period of 6.6 ms and a duty cycle of 15%. The transit time for ions to pass through the instrument has been calculated to be 68–75 μs for Ni^{1+} ions and 57–62 μs for Ar^{1+} ions with the equation presented by Bohlmark *et al* [16].

Time-resolved MS measurements have been conducted in a power-pressure matrix for a constant pressure of 13 Pa and varying RF power settings of 1000, 3000 and 4500 W as well as at a constant power setting of 4500 W and pressures of 3, 13 and 24 Pa.

2.1. Calculation of charge and impedance

The charge per pulse can be used as an indication of the actual power applied to the RF-coil. In equation (1), the charge (Q) is defined as the current (I) that passes through the circuit over a given time (t).

$$Q = I \times t. \tag{1}$$

As in this work the power is applied in a pulsed manner, the equation may be adapted to

$$Q_p = \sum_{0}^{t_{on}} I_s \times t_s, \tag{2}$$

where I_s is the current for the measurement step and t_s is the step size of the oscilloscope measurement. These values need to be summed up for the duration of the pulse on-time t_{on}.

The impedance in the coil can be used as an indicator for the influence of applied power on the impedance of the plasma.

The average impedance during the pulse can be calculated by summing up the calculation results for each measurement step and dividing this by the number of measurement points as expressed in equation (3).

$$Z_{avg} = \frac{V_{rms}}{I_{rms}} = \left(\frac{\sum_{n=t_{on}}^{t_{off}} V_n^2}{\sum_{n=t_{on}}^{t_{off}} I_n^2}\right)^{1/2} \text{[Ohm]}, \tag{3}$$

where Z_{avg} is the average impedance for the whole pulse period and V_n and I_n are the voltage and current for the individual oscilloscope measurement step respectively. As the phase response of the current and voltage probes is not known, this calculation results in a systematic error, which however is independent of plasma conditions and yields a reliable means of comparison. There is no significant phase change during the pulse on-time, and the power is negligible during the pulse off-time.

2.2. Plasma characterisation techniques

Analysis of the optical emission of the ICIS discharge was conducted by recording spectra by an OES monochromator (Jobin Yvon Triax 320, HORIBA Synapse CCD detector) with a spectral resolution of 0.12 nm. An optical fibre was placed *in vacuo* pointing to the cathode as indicated in figure 1. To protect the fibre from being coated, it was connected to a collimator assembly giving a spatial resolution of 10 mm.

In this study the optical emission of the plasma is correlated to the peak power applied to the coil. For this Ar, Cu, Ti and Ni neutral, single- and double-charged ions were analysed and compared to a model described by Dony *et al* [17], Rossnagel *et al* [10] and Pintaske *et al* [18], which was developed for DC and RF magnetron plasma processes and explains the correlation of power applied to the cathode to the plasma density, optical emission from Ar neutrals, metal neutrals and metal ions emission. The model predicts the emission intensity to be related to the applied power with a power law in which the exponent varies for different species depending on the number of collisions required to achieve the excited state that produced the emission. For example, the exponent for metal neutrals and metal ions would be two and three times that of the Ar neutrals respectively. The model assumes electron collision from the ground state to be the main excitation and ionisation mechanism. It neglects population from upper lying states due to their short life time. It assumes Corona equilibrium conditions considering a balance between collisional excitation and radiative decay.

At high pressure, a further ionisation mechanism that needs to be taken into account is Penning ionisation whereby metastable Ar atoms collide with metal neutrals and ionise them as the potential energy carried by the gas metastable neutrals of 11.55 eV [19] exceeds the ionisation potential of the metal. Rossnagel and Saenger [10] have described the density of sputtered material ionised by electron collision to be

$$n_{ion} = \alpha n_e^2 \text{SY} \int \sigma'_s \rho_e(E) v \text{d}E, \tag{4}$$

where SY is the sputter yield, σ'_s is the velocity dependant cross section for the species, $\rho_e(E)$ is the electron energy distribution, v is the electron velocity and α is a constant. As the ionisation of metal via a Penning collision requires similar collision path, the density of metal ions created through a Penning process can be assumed as shown in equation (5).

$$n_{ion}^{Penning} = \beta n_{sput} n_{Ar*} \int \sigma'_{Penning} \rho_{Ar}(E) v \text{d}E. \tag{5}$$

As the excitation of argon to the metastable state (Ar^*) by electron collision requires a similar collision path to that of the ionisation of the sputtered target material, the density of metastable argon can be assumed as

$$n_{Ar*} = \beta n_e n_{Ar} \int \sigma'_e \rho_e(E) v \text{d}E. \tag{6}$$

As Penning ionisation describes the ionisation of sputtered material by metastable gas collision, the electron density can be replaced by the metastable argon density in the equation resulting in a density of Penning ionised sputtered material of

$$n_{ion}^{Penning} = \beta n_{sput} n_e n_{Ar} \int \sigma'_{Penning} \rho_{Ar}(E) v \text{d}E \times \int \sigma'_e \rho_e(E) v \text{d}E \sim n_{sput} n_e C(T_e) \sim n_e^2 \text{SY} C(T_e), \tag{7}$$

where $\sigma'_{Penning}$ is the cross section of Penning ionisation for Ar and $C(T_e)$ is a constant related to the creation rate of metastable

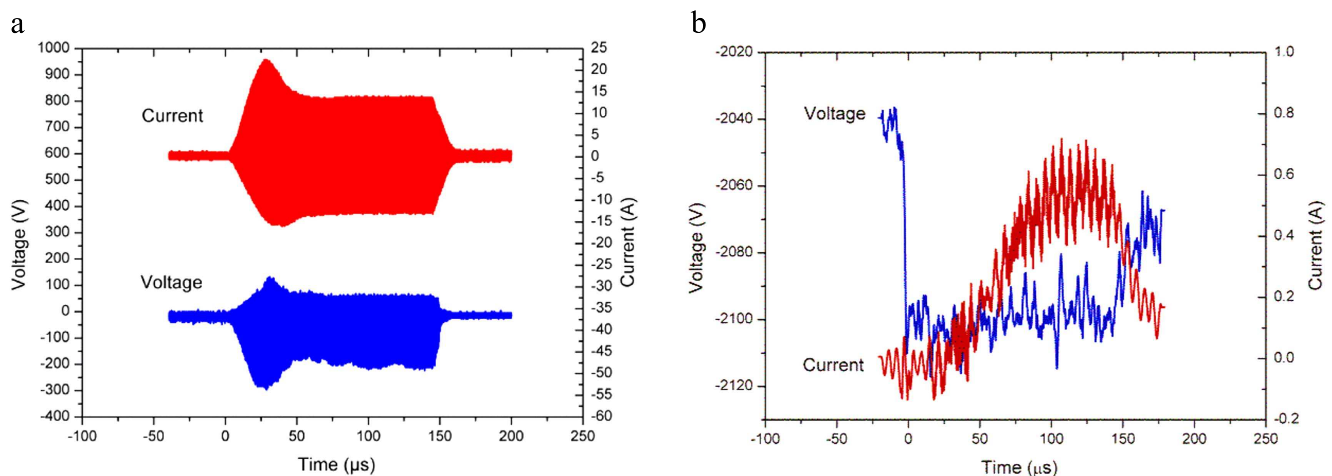

Figure 2. (a) Current and voltage waveform for a 2400 W ICIS titanium plasma with pulse width of 150 μs and frequency of 500 Hz applied to the coil. (b) Current and voltage measurement on the cathode.

Ar and rate of Penning ionisation which is dependent on the electron temperature T_e. As has also been shown by Mehdi *et al* [20], assuming the density of the sputtered species to be proportional to the electron density, from this equation it can be estimated that Penning ionisation can influence the intensity proportionally to n_e^2, which is identical to the two-step production mechanism involving sputtering and one electron collision.

Variations in the electron temperature within the experimental parameter range was estimated using the method proposed by Akatsuka *et al* [21], taking the line ratios of Ar I lines at 750.3869 nm (4p′$[1/2]_0$ with a wavenumber of 108.722 cm^{-1}) and 751.4201 nm (4p $[1/2]_0$ with a wavenumber of 107.054 cm^{-1}) which are highly sensitive to the electron temperature and weakly correlated with the plasma density.

To measure the mass and energy of the analysed species an energy resolved mass spectrometer (Hiden Analytical PSM 003) was used, sampling a volume near the substrate as shown in figure 1. The energy spectra resolution of the instrument is better than 0.5 eV.

3. Results

3.1. Current and voltage analysis

3.1.1. Current and voltage at the RF coil. Current and voltage waveforms for titanium in figure 2(a) show a transient behaviour within the initial 50 μs after the pulse is applied to the coil. During this time the voltage and current go through a maximum. After this initial spike, the current and voltage reduce to a level that remains constant for the remainder of the pulse.

In a similar fashion, the power signal (not shown) exhibits two distinct zones, the first being the initial 30 μs. The second zone from approx. 50 μs to the end of the pulse duration is an area where the power remains constant. In the case of 1000 W set power, the power in the initial phase is actually lower than the second phase. At higher set powers, the transient phase reaches higher levels than the rest of the pulse. This indicates that the transient is not part of the traditional glow discharge breakdown as weak plasma is already being formed in the first few μs of the pulse. The glow discharge breakdown would have already occurred earlier in the RF pulse.

In figure 2(b) the voltage applied to the cathode and the impeding ion current on the target are displayed. At the beginning of the pulse, the voltage rapidly decreases by 60 V and remains stable for the pulse on-time. When the pulse ends the voltage slowly reduces but is not fully discharged by the current. The current starts to increase after 30 μs of the pulse on-time and reaches a maximum of 0.6 A. The ion current peaks after 110 μs and is not sufficiently high to fully discharge the cathode.

The behaviour of the *I–V* waveforms is also confirmed by measurements that have been conducted by an Impedans Octiv VI probe. As can be seen in figure 3 showing the waveforms for an ICIS of Ti discharge. The voltage initially rises to a peak before reducing to a level which is sustained to the end of the pulse as the current rises. Further, as the current and voltage rise, the impedance drops to approx. 50 Ω.

Current and voltage are +70° out of phase before a pulse is applied due to a low power RF signal being delivered to the coil by the generator even in the off-times. The measured phase is consistent with capacitive coupling (E-mode) discharge. During the pulse the phase changes to +40° which is indicative of an inductive coupling in the discharge (H-mode). When the voltage is reduced and the current drops, the phase returns to +70° and capacitive coupling, but the impedance still remains constant and low and the current stabilises at a low level for about 180 μs. Following this, the impedance starts to rise, the current starts to drop towards 0 A and the phase jumps to +5°, gradually increasing and reaching +70° when the current reaches its minimum value.

3.1.2. Charge and impedance. The measured value for the charge in the RF coil, figure 4 (right *y*-axis), increases linearly

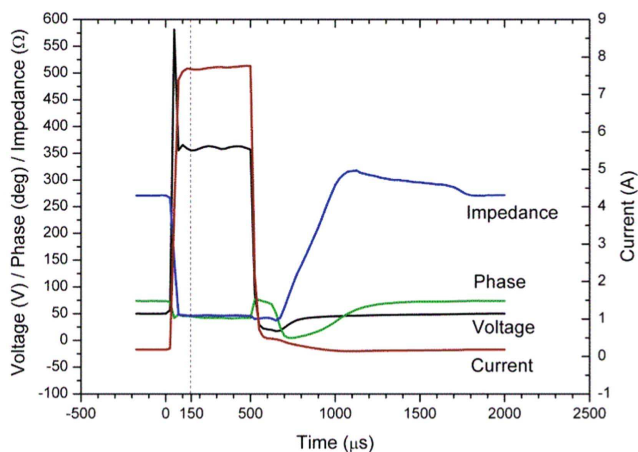

Figure 3. One titanium 2300 W ICIS pulse, 500 μs pulse width, 500 Hz repetition frequency. Voltage transient indicates the change from capacitive coupling to inductive coupling. Measurement was conducted by Impedans Octiv VI probe. The 150 μs mark, shows the pulse width of all other measurements in this work.

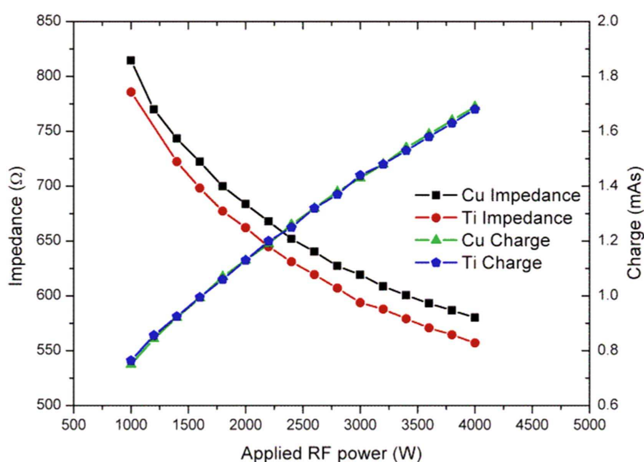

Figure 4. Average impedance (left y-axis) in the RF coil for copper and titanium during the pulse on-time. Charge (right y-axis) on the RF-coil with increasing applied RF power. For both materials, the charge increases linearly with increasing RF power.

with the set power. The deviation from linearity is around $-0.05‰$. Copper and titanium slopes are nearly identical. However the trends are similar. Average impedance in the coil during the pulse on-time, figure 4 (left y-axis), is reducing with increasing set power for copper and titanium. This decrease by 30% while the power applied to the coil is increasing fourfold is consistent with higher ionisation degree plasma created within the chamber.

3.2. Optical plasma analysis

Optical emission spectra show that the discharge contains excited gas neutrals, gas ions, metal neutrals and metal ions. The RF coil was supplied with RF power of 1000–4000 W at a constant process pressure of 13 Pa. OES results for nickel, figure 5, exhibit a linear increase for the initial 1000–2000 W set power in a log–log graph. Further, the slope is linear and

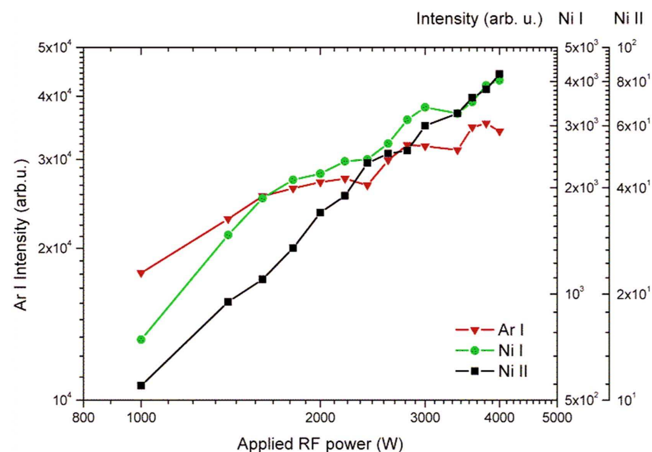

Figure 5. OES result for excited Ar neutrals (Ar I, 750.387 nm) correlating to the left y-axis, Ni neutral (Ni I, 310.188 nm) and Ni ion (Ni II, 333.188) lines correlated to the right y-axis.

the ratio between the argon and nickel neutral is approx. 2:1 and between argon and nickel ion is approx. 3:1 up to 4000 W set power. Slope values in table 2 show that there is only little deviation for Ar and Ni ions for different areas over the graph. The slope for Ni I is twice as steep and Ni II three times steeper than the Ar I slope. These slopes have been examined analogous to the model defined by Dony *et al* [17]. From this it is expected that the slopes for the metal species are twice as steep for metal neutrals and three times as steep as the slope of argon for metal ions. This shows that these results are comply the the modelling expectations.

For titanium all observed species (not shown), the slope is slightly steeper for the first two power settings. However for further increases the argon remains linear with a lower slope. For the metal species, compared to argon, there are some deviations from the straight linear increase. These deviations are within the error margin of the Ar line.

Comparing the result with the model, as can be seen in table 2, the slope for the Ti neutrals is about twice as steep as the argon slope. Ti ions also follow the model with a slope three times steeper than Ar.

In table 2, for copper, the slope for Ar is increasing linearly, while for the metal species there are two identifiable slopes. When considering the complete power range from 1000 to 4000 W, the measurements follow the model expectations very closely. However, when looking at the two slope ranges there is a difference in how the slopes of gas and metal species relate to each other. The slope at low power (1000–1600 W) does follow the model, albeit with a factor of 2 steeper slopes for the metal species. The origin of the factor 2 increase is discussed in detail in section 4. The slope in the higher power range (1600–4000 W) does not show any relation to the model.

3.3. Time averaged energy and mass spectroscopy

The ion energy distribution function (IEDF) for Ni^{1+} in figure 6, shows two peaks at low energy levels and one peak

Table 2. Comparisions of the slopes for different regions on the OES intensity graph for Ni, Ti and Cu.

Applied RF power	Ar I (750.387 nm)	Ni I (310.188 nm)	Ni II (333.188 nm)
1000–4000 W	0.44 ± 0.03	1.07 ± 0.08	1.45 ± 0.04
1000–2000 W	0.62 ± 0.06	1.63 ± 0.19	1.58 ± 0.07
2000–4000 W	0.41 ± 0.06	0.88 ± 0.07	1.23 ± 0.06
	Ar I (750.387 nm)	Ti I (363.546 nm)	Ti II (376.132 nm)
1000–4000 W	0.29 ± 0.01	0.73 ± 0.03	0.96 ± 0.05
1000–2000 W	0.32 ± 0.02	0.83 ± 0.11	1.23 ± 0.13
2000–4000 W	0.28 ± 0.01	0.78 ± 0.06	0.84 ± 0.08
	Ar I (750.387 nm)	Cu I (327.396 nm)	Cu II (455.592 nm)
1000–4000 W	0.37 ± 0.01	0.63 ± 0.06	1.07 ± 0.11
1000–1600 W	0.38 ± 0.02	1.48 ± 0.12	2.60 ± 0.15
1600–4000 W	0.35 ± 0.01	0.36 ± 0.02	0.64 ± 0.05

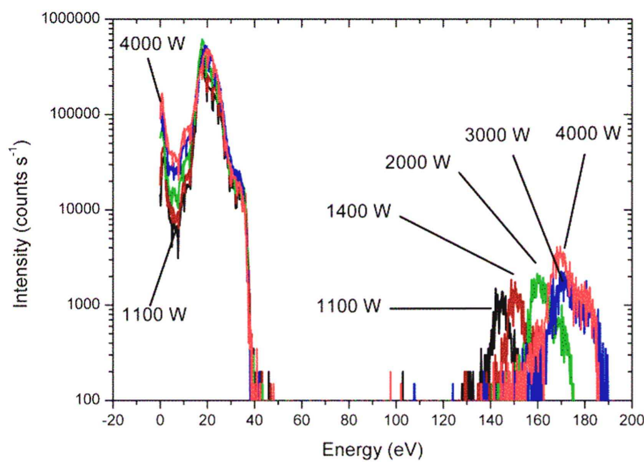

Figure 6. IEDF of Ni^{1+} ICIS plasma for increasing RF power with constant process pressure.

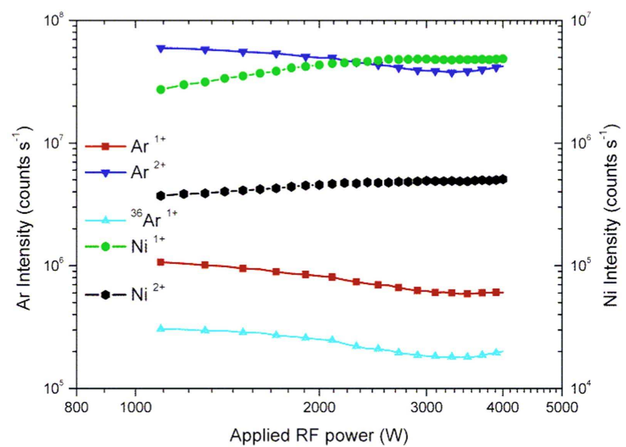

Figure 7. Integral of the MS intensity of a Ni ICIS plasma for increasing RF power with constant process pressure. The Ar^{1+}, Ar^{2+} ions and $^{36}Ar^{1+}$ isotope ion are correlated to the left *y*-axis and the Ni^{1+} and Ni^{2+} ions are correlated to the right *y*-axis.

at high energy levels. The first low energy peak appears at 1 eV and the signal increases with applied power. A second low energy peak at 20 eV shows a slight increase in plasma potential with increasing power. The high energy peak appears at 140 eV for 1100 W applied power, reaching a maximum of 170 eV for powers above 3000 W RF power.

The IEDF for Ti^{1+} (not shown) exhibits a low energy peak at 3 eV, increasing in intensity with applied RF power. The second low energy peak has the strongest intensity. It ranges from 20 eV reducing to 10 eV with increasing power. The peak also narrows from a width of 30 to 10 eV. Higher energetic peaks appear around 120 eV for 1400 W RF power, increasing to 160 eV for 4000 W RF power.

As in the previous cases, the IEDF for copper ions (Cu^{1+}) reveals two pronounced peaks at the low energy levels of 3 and 20 eV, with the 20 eV peak becoming narrower and shifting gradually to lower energy levels. Higher energetic ions are observed at 100 eV, which are related to the amplitude of voltage oscillations in the coil. The high energy peak appears at 140 eV and 160 eV as RF power increased to 2000 W and 4000 W respectively.

Integrating the IEDFs for each power setting we obtain the effect of increasing RF power on the ionisation degree in the plasma.

For Ni^{1+} and Ni^{2+} the integral intensities in figure 7 are increasing linearly with increasing set power up to 2200 W. For higher power settings the Ni ion intensities remain constant. Ar^{1+} and Ar^{2+} reduce linearly with increasing RF power from 1200 to 2100 W. In the range of 2100–3500 W, the Ar intensity is decreasing at a higher rate, before reaching a minimum at 3500 W. When increasing the RF power further, the Ar intensity increases again. This behaviour has been confirmed by measuring the isotope $^{36}Ar^{1+}$, which exhibits the same response.

In figure 8 the integral of the MS data shows a decrease for Ar^{1+} for increasing power RF power. Ar^{2+} initially rises reaching a maximum at 1600 W set RF power, before following the linear decrease with the Ar^{1+}. The reduction in intensity is probably caused by charge transfer.

Ti^{1+} and Cu^{1+} integral intensities rise linearly with increasing power, with the Cu^{1+} having a higher intensity for powers over 1400 W. The Ti^{2+} integral exhibits a general

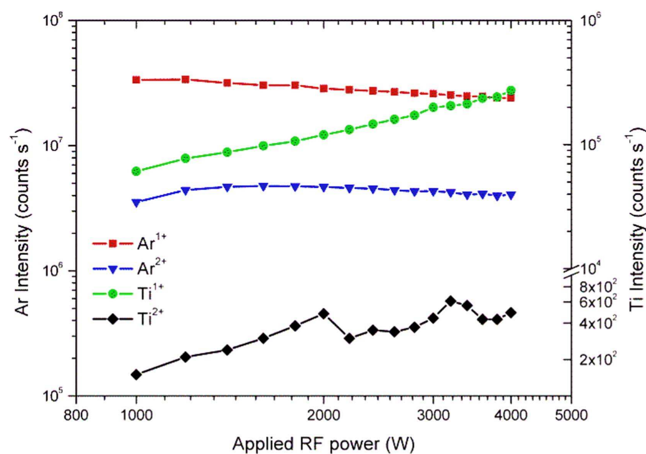

Figure 8. Integral of the mass spectroscopy intensity of Ar^{1+}, Ar^{2+} correlated to the left *y*-axis and Ti^{1+} and Ti^{2+} correlated to the right *y*-axis for increasing set RF power.

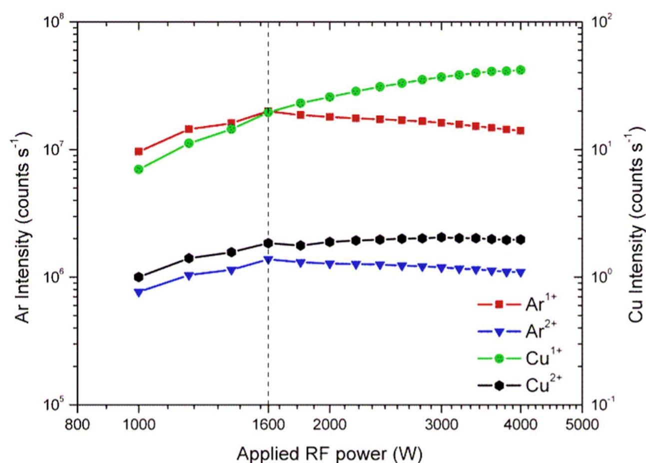

Figure 9. ICIS MS integral signal of Cu plasma. Ar^{1+} and Ar^{2+} is on the left *y*-axis, Cu^{1+} and Cu^{2+} on the right *y*-axis.

linear rise in intensity. Cu^{2+} intensity is decreasing logarithmically for increasing set power.

The integral of the MS signal for a Cu ICIS plasma for increasing set power to the RF coil in figure 9 shows a linear increase for all species for the set powers up to 1600 W. For higher powers, the Ar^{1+} and Ar^{2+} lines decrease linearly, while the Cu^{1+} continues to increase before the intensity saturates for powers above 4000 W. Cu^{2+} intensity does not change significantly for powers above 1600 W.

3.4. Time resolved energy and mass spectroscopy

Time resolved energy and mass spectroscopy of pulsed plasma processes gives an insight into the evolution of the plasma composition and ion energy over the whole pulse period. The pulse on-time, when the plasma source is on, exhibits the generation of process gas ions and sputtered metal ions. The pulse off-time exhibits the evolution of ion decay, when the plasma source is turned off.

In figure 10(a), the lowest pressure measurement of Ar^{1+}, three distinctive types of ion energy levels in the plasma are identifiable in two different temporal regions. The first region from 0–1 ms pulse delay, shows a broad energy spectrum from 1–180 eV with increased intensity in the 1–20 eV region and a high intensity peak at 160–180 eV.

The majority of ions in this region are fast, highly energetic ions with an energy of 160–180 eV originating from the coil area.

The high intensity peaks with an exponent of the order of 10^{+6} counts s^{-1} with low energy, are thermalised ions that are created near the spectrometer.

With increasing pressure (see figures 10(c) and (e)), this energy is reduced due to the reducing mean free path causing more collisional interactions and thus a reduction of energy, this is also visible in the case of nickel ions (figures 10(b), (d), (f)).

A second region between 1 and 6.6 ms, the bulk of the plasma, can be attributed to ions originating from the target and coil. With increasing process pressure the time the ions need to arrive at the spectrometer is increased due to an increased collision frequency. The plasma potential is between 10–30 eV for 3 and 13 Pa and 20 eV at 24 Pa. For Ni, at 3 Pa the majority of ions have an energy of 160 eV and a small bulk plasma. There is a large increase of bulk plasma intensity from 3 to 13 Pa. With increasing pressure the highly energetic ions reduce and the bulk plasma increases, showing a transformation from gas-dominated to metal-rich plasma from 1–5 ms. Due to the increased ion lifetime, the peak intensity is extended over the whole pulse period at the plasma potential.

For a constant pressure of 13 Pa and varied RF power of 1000, 3000 and 4500 W (figure 11), the influence of increasing energy is most clearly visible during the first millisecond. As in the pressure variation measurements, there are three ion types identifiable. Highly energetic, fast ions in the region of 140–160 eV, thermalised ions with an energy of 1 eV and the plasma potential at 20 eV. The energy of high energetic ions increases from 140 eV at 1000 W to 170 eV at 4500 W in line with an increased voltage driving the coil. The lifetime of ions and the intensity of ions at the plasma potential do not change with increasing power. While for all power settings the ion lifetime and peak intensity in the bulk plasma is homologous for both Ar and Ni respectively, for a power of 1000 W broader peak in the region of 10^{+5} counts s^{-1} ion flux is sustained beyond 4 ms compared to the higher power settings. This may be an indication of fewer collisions, hence extending the lifetime of the ions in the low power range. Further, the maximum energy of Ar^{1+} at 1000 W is 20 eV less that for the higher power settings.

The abrupt reduction in flux at energies slightly above the maximum flux signifies an ion population with low temperature. This is a result of the high pressures of operation and mean free paths which are small relative to the size of the coil. The ion population is shifted to high energy due to variations in plasma potential. The variations in plasma potential are closely linked to the application of power to the coil and their value is related to the magnitude of the voltage on the coil. As RF power is turned off, the voltage goes through a minimum and slowly increases to ~40 V throughout the pulse-off time

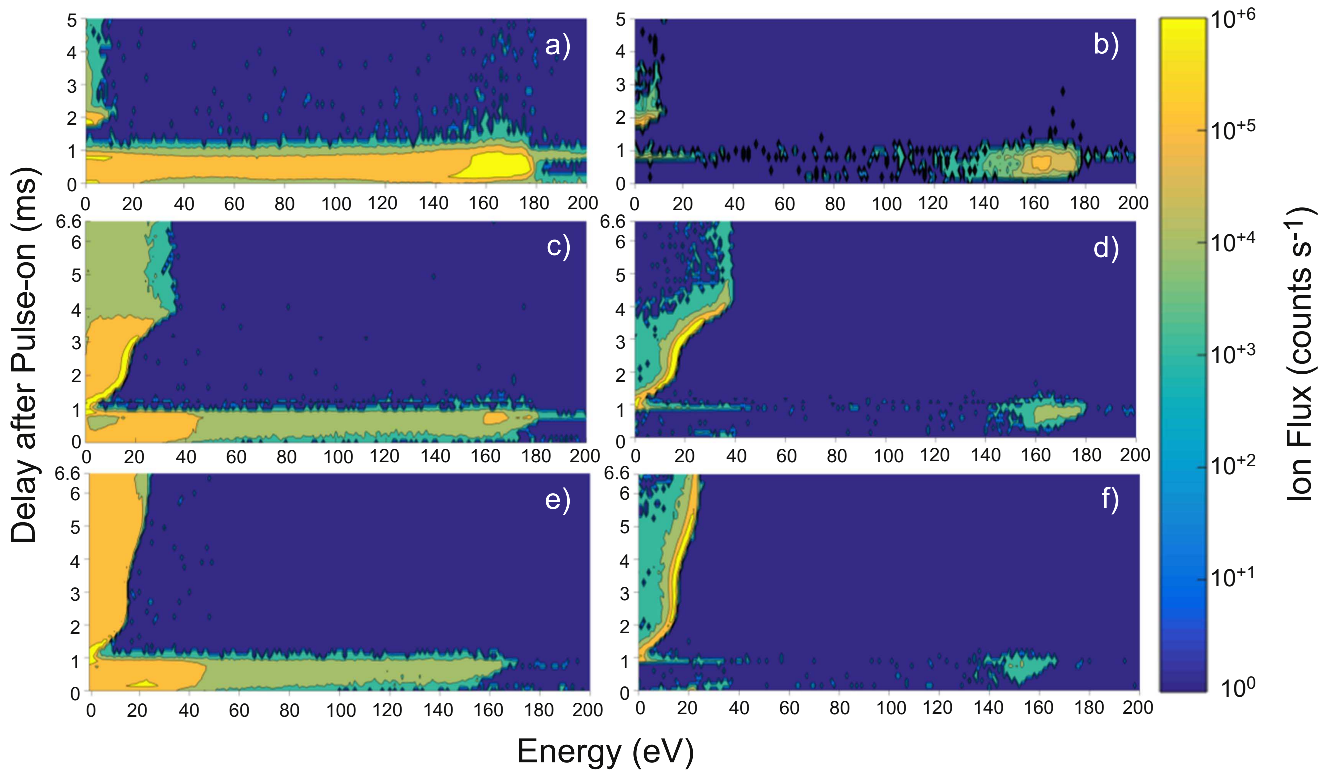

Figure 10. Time resolved MS of a 1 ms 150 Hz Ni ICIS pulse at a constant power of 4500 W. (a), (c) and (e) show the ion flux for Ar^{1+} and (b), (d) and (f) for Ni^{1+} for a pressure of 3 Pa, 13 Pa and 24 Pa respectively.

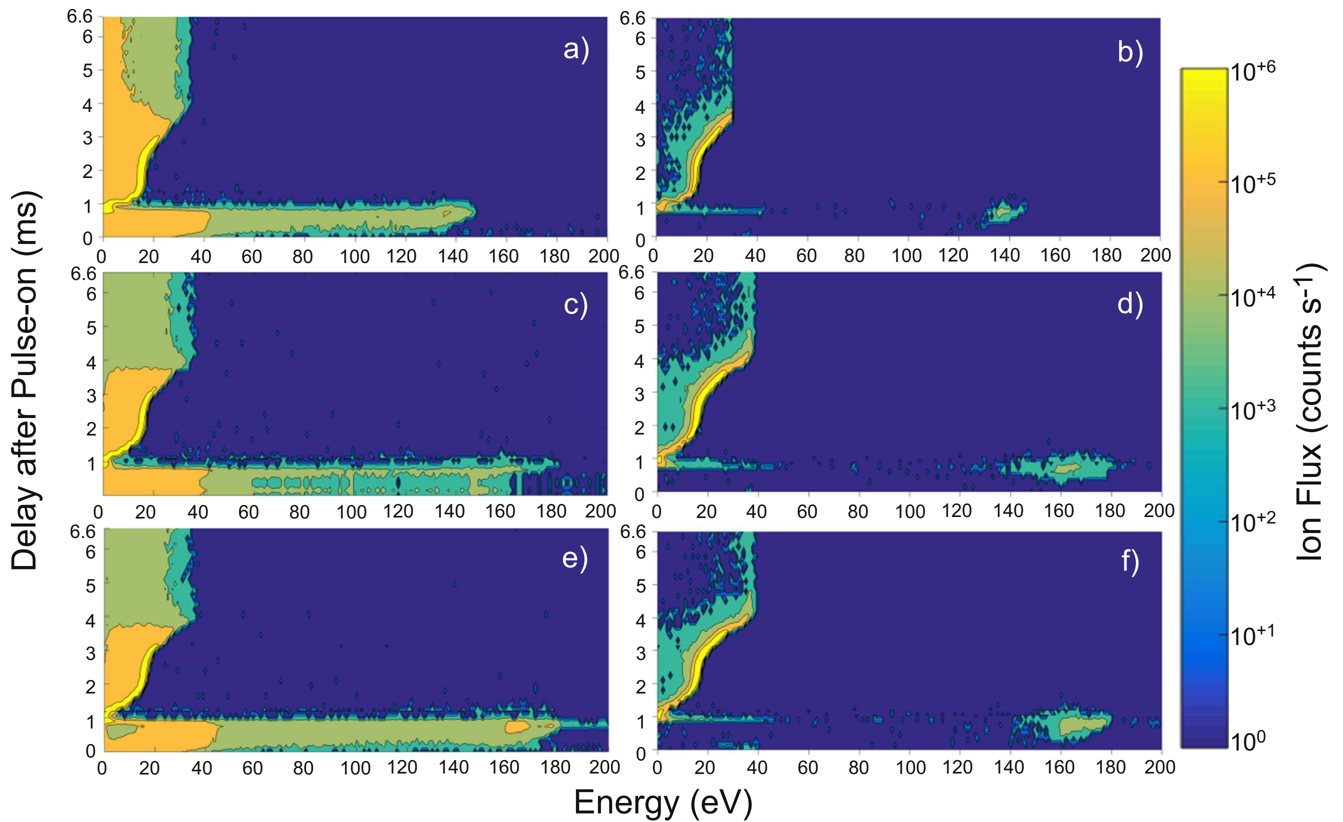

Figure 11. Time resolved MS of a 1 ms, 150 Hz Ni ICIS pulse at 13 Pa. (a), (c), (e) show Ar^{1+} and (b), (d), (f) show Ni^{1+} for 1000 W, 3000 W and 4500 W respectively. Ion flux is displayed in counts s^{-1} in log scale with the colour representing the magnitude of ion flux.

as seen in figure 3. This behaviour is mirrored in the plasma potential (figure 11) with ion energy peaking at 160 eV then reducing to a few eV and increasing again to ∼40 eV.

At pressures below 13 Pa the plasma decays completely within the period and it is ignited and developed by each application of the RF pulse. At higher pressures the plasma persists and combines with the new pulse.

Table 3. Slopes of the ICIS of Cu plasma for Cu and Ar ions as measured by mass spectroscopy.

Cu ICIS MS Slopes	1000–1600 W	1600–4000 W
Argon^{1+} (40 amu)	1.48 ± 0.21	−0.35 ± 0.02
Argon^{2+} (20 amu)	1.20 ± 0.14	−0.23 ± 0.01
Cu^{1+} (63 amu)	2.14 ± 0.13	0.82 ± 0.05
Cu^{2+} (31 amu)	1.26 ± 0.17	0.10 ± 0.03

4. Discussion

From figure 2 it can be seen that the current and voltage waveforms of an ICIS discharge show a strong similarity to the ICP discharges described by Guo and DeJoseph [15]. The initial peak in voltage is described as a feature of the power supply which cannot react fast enough to reduce the voltage and follow reduction in impedance. Further measurements with an Impedans OCTIV VI probe have given a clear indication that the main energy coupling is inductive. The coupling switches from capacitive to inductive within a few microseconds of applying the voltage indicating an efficient ionisation of the gas and quick rise in plasma density. On the other hand, the decay of plasma is relatively slow due to the low cross section of three-body recombination and the slow diffusion of ions to the walls given by the high operating pressures. The rapid switch off of voltage at the end of the pulse leaves a high density plasma driven by a small voltage field, preserving the inductive coupling for some 180 μs. The collapse of plasma density and current leads to a switch to capacitive coupling during which the plasma is purely resistive.

The impedance of the coil reduced with increasing applied power (figure 4) indicating a inductive portion of the discharge which is reduced by the applied power. The linear increase in the total charge within the pulse indicates that the increasing energy is absorbed efficiently by the plasma and the actual power is proportional to the power set at the power supply indicating a stable and controlled process.

The comparison of Ti and Ni OES results with the model shows that these materials adhere very well to the expected result. As has been discussed in more detail in Loch *et al* [22], in a log–log graph, the slope for metal neutrals is twice as steep as the gas slope and for metal ions it is three times as steep.

As one electron collision is necessary to excite the gas and a further electron collision needed to excite the metal atom, it can be concluded that the density of excited metal atoms and the intensity of light emission are proportional to the density of electrons squared n_e^2. To ionise the metal atoms, a further electron collision is needed and the intensity is related to n_e^3. The plasma density is related to the power and emission intensity of Ar neutrals through $P_{RF} \sim n_e^{\beta} \sim I_{ArI}^{\beta}$ [17]. According to the experimental data, the exponent β is in the range 0.3–0.4 for Ni, Ti and Cu discharges utilising Ar as process gas.

The good fit of the data for ICIS of Ti and Ni to the described model illustrates that its assumptions are a good approximation to the actual phenomena. In this context, at a constant process pressure the results suggest that the creation of ions by electron collisions or Penning ionisation is balanced by charge exchange and out diffusion towards the anode (chamber walls) and subsequent absorption or neutralisation. Among other things, this signifies similar out-diffusion rates for metal neutrals and metal ions.

For Ti and Ni and for Cu above 1600 W, a reduction in Ar^{1+} signal of approximately 50% is observed which could be attributed to heating and rarefaction of the gas by the coil and is countered by an increase in electron temperature. The reduction was the same regardless of sputter yield of the material indicating that cooling of the electron temperature by metal vapour was a minor effect. Rossnagel [23] has shown that energising the coil leads to a reduction of gas density due to heating of the gas by collisions with atoms sputtered from the coil and by charge exchange with ions that have been accelerated either by the potential drop in the presheath or by elastic collisions with electrons. The measured density reduction was as much as 60% for coil power density of up to 1 W cm^{-2}. Further gas heating could come from the sputtered flux from the cathode—according to estimates by Dickson *et al* [24] sputter particle densities equivalent to 1% of the gas particle density are sufficient to cause rarefaction in excess of 40%. Extrapolating to the densities of the current experiment of 100 W cm^{-2}, and considering plateauing at high powers, the reduction is estimated to be up to 70% if the power is delivered continuously or in case of pulsing; the reduction is likely to be less.

The ICIS of Cu discharge differs from the Ti and Ni cases. Up to 1600 W applied power there is a steep increase in optical emission and ion flux detected by mass spectroscopy. Both diagnostic methods report similar slopes for the flux of Cu^{1+} ions and their emission line intensity for Cu II of 2.14 and 2.6 respectively indicating a minor lowering of electron temperature within the studied range of RF powers and a good correlation between the emission intensity and number density for all species Cu II, Cu I and Ar I.

It is noteworthy that the slope for the Ar^{1+} flux (table 3) is factor two greater than anticipated from the emission of Ar I (table 2) and the expected doubling of the slope for Ar II to 0.76. This suggests a multi-step process of ionisation for argon involving excitation and ionisation of the excited state, which relates the density of Ar^{1+} ions to the electron density n_e to the power of 2 or even 3 and to P_{RF} to the power of 2β or 3β. It is reasonable to expect that multi-step ionisation would proceed via the Ar metastable states which are long-lived [25]. Such processes are favoured at high pressure due

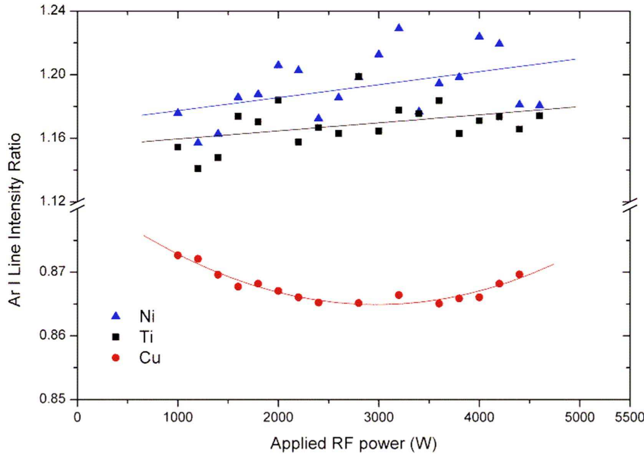

Figure 12. Ratio of the optical emission intensity of Ar neutral lines with different energy levels indicating a rise of electron temperature with increasing set RF power for Ti and Ni and a reduction for Cu. Energy levels were retrieved from the ViZier Database [30].

to the slower loss rates to the walls of the chamber and longer lifetime of excited states in the bulk plasma. They are also favoured at high plasma density where electron collision frequencies are high. Calculations [26] suggest that a two-step ionisation may prevail over a single-step process at pressures of >3 Pa and plasma density of 10^{12} cm^{-3}.

Measurements [27] have demonstrated the prevalence of excitation over ionisation at pressures of >1.3 Pa and a wide range of powers. The ICIS plasmas described in these studies are above these boundaries.

The multi-step ionisation of Ar may be brought about by the higher sputtering yield of Cu which effects a high metal vapour density that cools down the electrons. Estimates of T_e based on emission line ratios in figure 12 clearly show that Cu sustains much lower electron energies than the lower sputter yield Ti and Ni. It is also evident that the type of sputter material has a greater influence on T_e than the power applied to the coil. This may warrant a different ionisation mechanism of Ar in Cu compared to Ti and Ni and could explain the contrasting influence of coil power which in the case of Cu increases Ar^{1+} flux and in the case of Ti and Ni has the reverse effect.

The production of Cu vapour is completely accomplished by sputtering by Ar^{1+} ions which dominate the content of the plasma and exceed several-fold self-sputtering rates by Cu^{1+}. The rate of ionisation of Ar^{1+} directly impacts the rate of the sputtering process and the production of Cu vapour with

$$[\mathrm{Cu}^0] = Y[\mathrm{Ar}^{1+}] \sim P_{\mathrm{RF}}^{2\beta}, \quad (8)$$

where Y is the sputter yield and $n_{\mathrm{Ar}+}$ is the density of Ar^{1+} ions, which in this case has a different relation to the applied power than the density of electrons due to the multi-stage ionisation process of Ar. This may explain the factor 2 steeper than predicted slope for Cu I emission. It also indicates a steep increase in Cu sputter rate for a moderate increase in applied RF power.

The Cu II emission may be produced by ions that are created through a multistep process for Cu. Cu has two metastable states, $3d^9 4s^2\ {}^2D_{5/2}$ (1.39 eV) and $3d^9 4s^2\ {}^2D_{3/2}$ (1.64 eV) which are long lived. They may be populated from excited levels and subsequently ionised as described in equations (9)–(10). The creation of Cu metastables itself could proceed in a multi-step fashion with a sequence of excitation collisions followed by decay to a metastable energy level. Taking into account these reactions, the emission intensity of the Cu ion to the applied RF power can be expressed by equation (11) for excitation and ionisation by electron impact.

$$e + Me^0 = Me_m^* + e, \quad (9)$$

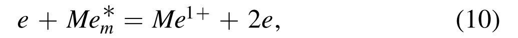

$$e + Me_m^* = Me^{1+} + 2e, \quad (10)$$

$$\log I_{\mathrm{Cu}^{1+}} \sim \log([Me_m^*]n_e) \sim \log([Me^0]n_e^m n_e)$$
$$= \log(P_{\mathrm{RF}}^k P_{\mathrm{RF}}^{(m+1)\beta}) = (k + (m+1)\beta)\log P_{\mathrm{RF}}. \quad (11)$$

Equation (11) shows that Cu ionisation by electron impact would result in a slope of $k + (m + 1)\beta$, where k is the slope for Cu I and $m = \{1, 2\}$ is the number of collisions required to create a Cu metastable. Taking k as 4β from table 2 the overall slope for Cu II would be between 6β and 7β equivalent to a range of slopes between 2.28 and 2.66 which fits well with the experimentally observed values. In comparison Ni metastables are close to ground with <0.4 eV requiring a similar ionisation energy. Ti does have high-energy metastables, however it also has a factor of 3 lower sputter rate than Cu leading to a lower density and collision probability. This suggests that multistep metal ionisation is favoured when long-lived metastables are highly energetic and are present in high numbers.

Eventually, when power levels exceed 1600 W, the increasing plasma density may drive the intermediate Ar states to a saturation above which the ionisation rate is independent of n_e [25] leading to a steady production of gas ions.

The increasing current through the coil may lead to a reduction in the efficiency of power transfer [28] and associated slowing of ionisation processes. The continual injection of sputtered metal into the plasma results in the reduction of T_e observed in figure 12 which may induce the observed reduction in the fluxes of Ar^{1+} and Ar^{2+} ions and Ar I intensity. Self-sputtering by Cu^{1+} may still sustain the production of Cu atoms and maintain the increase in Cu ion flux observed in figure 9. This is countered by the reduced T_e and diminished sputtering by Ar^{1+} and eventually leads to saturation, first for the double charged ion and subsequently to the single charged ions.

Penning ionisation is a concomitant route for metal ion production. As discussed earlier in section 2.2, for high process pressures Penning ionisation may also lead to a scaling of the Cu^{1+} flux on n_e^2. As in ICIS the process pressures are ⩾3 Pa, an increased Ar metastable ratio is likely. Single step ionisation and Penning ionisation are not distinguishable in the modelling results.

As can be seen in table 2, at the lower power range (1000–1600 W), the slopes of the metal neutrals and ions are a factor of two greater than the model predicts. Additional Penning ionisation contributing to the election collision

ionisation would not change the slope of the metal species. The argon slope is not influenced as the surveyed Ar lines are not metastable. The main factor that can increase the slope is additional electron collisions. For this reason multi-step excitation and ionisation is most likely the cause of the increased slope in this power range.

Table 3 shows that the slopes of the Cu^{1+} MS integral are steeper than the Ar^{1+} slopes indicating increasing metal ion content in the plasma. Sputtering of the coil may provide a second source of Cu optical emission which may be substantial due to the high sputter yield of copper. In comparison, for Ti and Ni plasma, it has been observed that the coil is coated by the target material. Resputtering of Ti and Ni from the coil does not seem to have an effect on the plasma due to the lower sputter yields of these elements.

A possible reason for the reduced flux of Ar^{1+}, Ar^{2+} and Cu^{2+} ions with RF power could be a reduced efficiency of ionisation due to cooling of the electron temperature and gas rarefaction. An estimate of the electron temperature is displayed in figure 12 and shows a cooling trend with RF power, which may be responsible for the reduction in Ar^{1+}, Ar^{2+} and Cu^{2+} flux. Experiment and model calculations by Dickson *et al* [25] and Nichols *et al* [29], have demonstrated a reduction in electron temperature with magnetron power due to the presence of metal vapour with considerably lower ionisation potential than argon. In the current experiment, increasing RF power also increases the flux of plasma to the target and increases the flux of sputtered particles.

Due to the lower sputter yield of Ni and Ti, thus a lower density of sputtered material in Ni and Ti plasma compared to the Cu plasma, the respective electron temperatures are greater than that of Cu. For both Ni and Ti, the intensities of the metal ion counts are increasing, while the Ar ion intensities are decreasing, creating increasingly metal ion rich plasma with increasing RF power.

The IEDFs for all three examined materials exhibit pronounced high intensity peaks at low energies in the range of 10–20 eV. This is in line with conventional ICP-MS [31]. It is accepted, Petrov *et al* [32], that these low energetic ions can produce dense coatings provided there is a sufficiently high ion-to-neutral flux. It has been demonstrated, Loch *et al* [23], that the high ionisation degree combined with the moderate ion energy in ICIS results in high density and low lattice defect films with magnetic behaviour. With its unique characteristics of the deposition flux compared to magnetic I-PVD techniques, ICIS enables the generation of highly ionised plasma with magnetic materials with a higher ionisation degree than HIPIMS, as demonstrated in Loch and Ehiasarian [33]. A comparison with HIPIMS shows the lower energy level increases from approx. 4–5 to 20 eV.

5. Conclusions

This study has demonstrated an inductive coupling to the plasma when high peak RF power levels are used during the pulse on-time.

Conducting large RF currents in the coil creates a magnetic field perpendicular to the target surface, which counteracts the weakening of plasma confinement normally associated with the quenching of the magnetic field by the magnetic target materials in conventional I-PVD magnetron processes. Thus, sufficient numbers of electrons are confined inside the coil area enabling the excitation and ionisation of gas and metal species. Sputtering of nickel experiments have demonstrated that this enables the generation of highly ionised plasma of a magnetic material, comparable to non-magnetic materials such as copper and titanium, with conventional I-PVD magnetron processes.

By applying the OES data to a model linking the emission intensity to the power applied to the coil, it has been demonstrated that the main excitation and ionisation mechanisms for metal species are single-step electron impact collisions. An unexpected enhancement in ionisation efficiency was observed for copper, where multi-step electron ionisation processes are favoured over Penning and single-step due to a high sputter yield and long-lived metastable states.

The measured time averaged ion energy of 20 eV enables the deposition of high quality magnetic coatings with dense microstructure on complex-shaped surfaces as this energy level stimulates surface mobility whilst remaining under the threshold for lattice defects and stress generation.

Acknowledgements

We would like to thank Impedans Ltd for the provision of the OCTIV VI probe. This work was partially supported by the Engineering and Physical Sciences Research Council under grant number EP/J011398/1.

References

[1] Rossnagel S M and Hopwood J 1993 Magnetron sputter deposition with high levels of metal ionization *Appl. Phys. Lett.* **63** 3285–7

[2] Kouznetsov V, Macák K, Schneider J M, Helmerson U and Petrov I 1999 A novel pulsed magnetron sputter technique utilizing very high target power densities *Surf. Coat. Technol.* **122** 290–3

[3] Window B and Sharples F 1985 Magnetron sputtering sources for ferromagnetic material *J. Vac. Sci. Technol.* A **3** 10–3

[4] Fan Q and Chen H 1993 Effects of magnetic field on the target erosion in the symmetrical magnets magnetron sputtering method *Thin Solid Films* **229** 143–5

[5] Huang S, Cheng Q J and Ostrikov K 2010 Inductively coupled plasma-assisted RF magnetron sputtering deposition of boron-doped microcrystalline Si films *J. Alloys Compd.* **499** 166–70

[6] Godyak V A 2003 Plasma phenomena in inductive discharges *Plasma Phys. Control. Fusion* **45** A399

[7] Joo J 2000 Ionization enhancement in ionized magnetron sputter deposition *J. Vac. Sci. Technol.* A **18** 23–9

[8] Jang D-S, Jung S-J and Lee J-J 2012 Al doped zinc oxide thin films on polymer substrates deposited by inductively coupled plasma assisted reactive sputtering *Curr. Appl. Phys.* **12** (Suppl 4) S118–22

[9] Hopwood J and Qian F 1995 Mechanisms for highly ionized magnetron sputtering *J. Appl. Phys.* **78** 758–65

[10] Rossnagel S M and Saenger K L 1989 Optical emission in magnetrons: nonlinear aspects *J. Vac. Sci. Technol.* A **7** 968–71

[11] Gudmundsson J T 2008 Ionization mechanism in the high power impulse magnetron sputtering (HiPIMS) discharge *J. Phys.: Conf. Ser.* **100** 082013

[12] Loch D A L and Ehiasarian A P 2012 A novel sputtering technique: inductively coupled impulse sputtering (ICIS) *IOP Conf. Ser.: Mater. Sci. Eng.* **39** 012006

[13] Rossnagel S 2000 Ionisation by radio frequency inductively coupled plasma *Thin Films* **27** 37–65

[14] Müller K-H 1987 Ion-beam-induced epitaxial vapor-phase growth: a molecular-dynamics study *Phys. Rev.* B **35** 7906–13

[15] Guo W and Dejoseph C A JR 2001 Time-resolved current and voltage measurements on a pulsed rf inductively coupled plasma *Plasma Sources Sci. Technol.* **10** 43

[16] Bohlmark J, Lattemann M, Gudmundson J T, Ehiasarian A P, Aranda Gonzalvo Y, Brenning N and Helmersson U 2006 The ion energy distributions and ion flux composition from a high power impulse magnetron sputtering discharge *Thin Solid Films* **515** 1522–6

[17] Dony M F, Ricard A, Dauchot J P, Hecq M and Wautelet M 1995 Optical diagnostics of d.c. and r.f. argon magnetron discharges *Surf. Coat. Technol.* **74-75** 479–84

[18] Pintaske R, Welzel T, Schaller M, Kahl N, Hahn J and Richter F 1998 Spectroscopic studies of a magnetron sputtering discharge for boron nitride deposition *Surf. Coat. Technol.* **99** 266–73

[19] Minnhagen L 1973 Spectrum and the energy levels of neutrsdaoal argon, Ar I *J. Opt. Soc. Am.* **63** 1185–98

[20] Mehdi T, Legrand P B, Dauchot J P, Wautlet M and Hecq M 1993 Optical emission diagnostics of an rf magnetron sputtering discharge *Spectrochim. Acta* B **48** 1023–33

[21] Akatsuka H, Tanaka E, Ando K, Nezu A, Kuwahara D and Shinohara S 2015 Approximate monitoring of electron temperature and density of argon-based plasma by line-intensity ratio measurement with collisional radiative model *Proc. 2015 Int. Symp. on Dry Process* (The Japan Society of Applied Physics) pp 95–6

[22] Loch D A L, Aranda Gonzalvo Y and Ehiasarian A P 2015 Nickel coatings by inductively coupled impulse sputtering (ICIS) *Surf. Coat. Technol.* **267** 98–104

[23] Moisan M and Pelletier J 2012 *Physics of Collisional Plasmas* (Dordrecht: Springer) p 413

[24] Rossnagel S M 1998 Interaction between gas rarefaction and metal ionization in ionized physical vapor deposition *J. Vac. Sci. Technol.* B **16** 3008

[25] Dickson M, Qian F and Hopwood J 1997 Quenching of electron temperature and electron density in ionized physical vapor deposition *J. Vac. Sci. Technol.* A **15** 340

[26] Lee M-H and Chung C-W 2005 Effect of multistep ionizations on the electron temperature in an argon inductively coupled plasma *Appl. Phys. Lett.* **87** 131502

[27] Godyak V A, Piejak R B and Alexandrovich B M 2002 *Plasma Sources Sci. Technol.* **11** 525

[28] Chabert P and Braithwaite N 2011 *Physics of Radio-Frequency Plasmas* (Cambridge: Cambridge University Press) p 251

[29] Nichols C A, Rossnagel S M and Hamaguchi S 1996 Ionized physical vapor deposition of Cu for high aspect ratio damascene trench fill applications *J. Vac. Sci. Technol.* B **14** 3270

[30] Ochsenbein F, Bauer P and Marcout J 2000 *Astron. Astrophys. Suppl. Ser.* **143** 23–32

[31] Li Z, Miyake S and Mori M 2003 Plasma properties and ion energy distribution in DC magnetron sputtering assisted by inductively coupled RF plasma *Japan. J. Appl. Phys.* **42** 7086–90

[32] Petrov I, Barna P B, Hultman L and Greene J E 2003 Microstructural evolution during film growth *J. Vac. Sci. Technol.* A **21** S117

[33] Loch D A L and Ehiasarian A P 2016 Study of the effect of RF-power and process pressure on the morphology of copper and titanium sputtered by ICIS *Surf. Coat. Technol.* accepted (https://doi.org/10.1016/j.surfcoat.2016.10.018)